



Ultrasound-assisted preparation of chitosan/nano-silica aerogel/tea polyphenol biodegradable films: Physical and functional properties

Zhijun Wu^{b,1}, Yang Li^{a,1}, Jing Tang^{a,1}, Derong Lin^{a,1,*}, Wen Qin^{a,*}, Douglas A Loy^c, Qing Zhang^a, Hong Chen^a, Suqing Li^a

^a College of Food Science, Sichuan Agricultural University, Ya'an 625014, China

^b College of Mechanical and Electrical Engineering, Sichuan Agricultural University, Ya'an 625014, China

^c Department of Chemistry & Biochemistry, University of Arizona, Tucson, AZ 85721, USA

ARTICLE INFO

Keywords:

Chitosan
Nano-silica aerogel
Ultrasound-assisted
Biodegradable film
Antimicrobial property

ABSTRACT

In this study, chitosan(CS), nano-silicon aerogels(nSA) and tea polyphenols(TP) were used as film-forming materials and processed with ultrasonication to form films using the tape-casting method. The effects of ultrasonication time, temperature and frequency on the properties of CS/nSA/TP film were explored via material property testing. The results of response surface showed that the maximum tensile strength of the film was 4.036 MPa at ultrasonication time(57.97 min), temperature(37.26 °C) and frequency(30 kHz). The maximum elongation at break of the film was 279.42 % at ultrasonication time(60.88 min), temperature(39.93 °C) and frequency(30 kHz). Due to cavitation and super-mixing effects, ultrasonication may make the surface of the film smoother and easier to degrade. After ultrasonication, TPs were protected by the 3D network structure composed of CS and nSA. Ultrasonication improved the antioxidant and antibacterial properties of the film. These results show that ultrasonication is an effective method to improve the properties of films.

1. Introduction

Petroleum-based plastics are widely used due to their good processing and excellent physicochemical properties. However, they cause great harm to the environment because they do not easily degrade. With the increasing concern for food quality and safety while reducing environmental pollution, seeking greener, environmentally friendly, and safe packaging materials have become a frontier hotspot in the field of food materials [1]. According to their composition, the natural biomaterials commonly used to prepare edible and biodegradable films include polysaccharides, proteins, lipids, and combinations of these components [2]. Among these materials, polysaccharides are known for their complex structures and diverse functions.

Chitosan (CS) is a chitin deacetylation derivative, a 2-aminodeoxy-β-D-glucan linked by a linear polysaccharide (1, 4), which is one of the most abundant polysaccharide found in nature after cellulose. CS has good physicochemical properties, such as film-forming capacity, moisture retention and biodegradation [3]. Due to its antibacterial activity, CS has huge application potential in antibacterial packaging. Many

studies have proven that CS-based films and coatings are effective in food preservation [4]. It is worth mentioning that it has the advantage of combining functional substances [5]. However, some problems, such as weak mechanical properties, poor water resistance, and poor thermal stability, must be resolved for the practical application of CS-based films [6].

In the past few years, composite films formed by nanomaterials have been extensively studied due to their ability to significantly improve the performance of polymers when compared with the use of polymers alone. Potential improvements include enhanced mechanical strength, heat resistance, and barrier properties of the films [7]. The nano-silicon aerogel (nSA) is a porous material composed of nano-silica particles with a three-dimensional (3D) network structure and good transparency. It has many remarkable characteristics, including low density, high specific surface area, extremely high porosity, excellent high temperature resistance and hydrophobicity, which is hoped to improve the physicochemical of edible films by forming cross-links between biopolymers (such as polysaccharides and proteins). Aragon-Gutierrez et al. [8] added nSA to polylactic acid to form a degradable film, which effectively

* Corresponding authors.

E-mail addresses: lindr2018@sicau.edu.cn (D. Lin), qinwen@sicau.edu.cn (W. Qin), daloy@arizona.edu (D.A. Loy).

¹ These authors contributed equally to this work.

improved the thermal stability, mechanical properties and barrier properties of the film. In our previous research [9], similar results have been obtained. CS and nSA have good compatibility, and there is an interaction between them. Although CS/nSA is a promising biopolymer for active food packaging, it has no significant antioxidant activity (about 2.05 %). Therefore, improving its antioxidant activity can expand its application in active food packaging [10].

Tea polyphenols (TP), which are a polyphenol compound with extremely high antioxidant activity extracted from tea, contain catechins (about 60 % ~ 80 %), flavonoids, anthocyanins and phenolic acids. Among them, catechins mainly include epigallocatechin gallate (EGCG), epigallocatechin (EGC), epicatechin gallate (ECG) and epicatechin (EC), resulting in their multiple functions, such as anti-cancer and anti-bacterial effects [11]. The antioxidant mechanism of polyphenols is principally attributed to their ability to capture active oxygen and chelate metal ions, which could generate free radicals through the Fenton reaction [12]. Hydroxyl groups in phenolic compounds can interact with the cell membrane of bacteria, destroy the structure of cell membrane, and lead to leakage of cell components. Those are the preferred choice for the preparation of active packaging films to prevent lipid oxidation and microbial spoilage in food [13]. Liu et al. [14] integrated TPs into CS and found a strong interaction between them. The addition of TPs can significantly increase the antioxidant activity of the CS film, while reducing the water vapor permeability (WVP) of the film. Furthermore, Zhang and Jiang [15] also obtained similar conclusions and the mechanical and anti-bacterial properties of the composite films were improved when adding TP-silver nanoparticles to CS.

Generally, when preparing a film-forming solution, nanoparticles tend to form agglomerates that are difficult to break, and it is necessary to stir the heterogeneous biopolymer aggregates or particles sufficiently to form a uniform matrix of the film during water evaporation [16]. In recent years, ultrasound technology has been increasingly used to solve blending problems. Ultrasound involves the formation, growth and implosion of tiny bubbles or cavities in biopolymer suspensions, which can cause the poorly flowing polymer to split into smaller pieces [17]. In addition, ultrasound can also produce strong thermal, mechanical, super-mixing and cavitation effects, such that the original hydrogen bonds and hydrophobic bonds in the medium break [13]. This action leads to the formation and exposure of more reaction centers, accelerating the speed of chemical reactions, and enabling macromolecules to recombine with each other to form various non-polar bonds. As a result, the physicochemical properties of the film can be further improved to some extent. Liu et al. [18] found that ultrasonic treatment can make the corn starch polymer film have better stretch and moisture resistance. However, long-term intense ultrasonic treatment will destroy the structure of the polymer to a certain extent. Similarly, Liang et al. [19] confirmed that with the increase of the ultrasonication time, the mechanical and barrier properties and of the film increased, but it has no significant effect on other properties. In addition, Liu et al. [13] believed that ultrasonic treatment improved the barrier properties and degradability of polyvinyl alcohol (PVA)/TPs films, and the antibacterial rate of the films against *E. coli* and *S. aureus* was increased. A large number of studies have confirmed that the application of ultrasonic technology can modify the composite films. However, there are relatively few studies on the effect of ultrasonic treatment on the physicochemical properties of composite films.

The aim of this study was to investigate a composite film for food packaging with good mechanical, anti-oxidation and antibacterial properties, and to provide an environmentally friendly and biodegradable film material for the food packaging industry. Therefore, we hypothesized that the addition of TP could significantly improve the oxidation resistance of the film, and the film with the best mechanical properties could be prepared through ultrasonic cavitation effect. On this basis of the film, the effect of ultrasonic technology on the antioxidant, antibacterial and biodegradability of a series of CS-based films were studied. These results fill the gaps in the literature and highlight

the role of ultrasonic treatment in improving the performance of active packaging materials.

2. Materials and methods

2.1. Materials

Chitosan—of food grade, with a ≥ 90 % degree of acetylation, and a molecular weight of approximately 100 kDa—was purchased from Weijia Food Additive Co., Ltd. (Zhuhai, China). Tea Polyphenols (98 % purity) were supplied by Sanhua Biological Technology Co., Ltd. (Henan, China). Nano-silicon aerogel (Nano-component: 98 %, thermal conductivity: 0.013 W/m K, density: 40 g/cm³, specific surface area: 600–1000 m²/g) was supplied by Langfang Yuao Energy Saving Technology Co., Ltd. (Shanxi, China). Glacial acetic acid (Analytical reagent) was obtained from Zhengzhou Kangqun Biotechnology Co., Ltd. (Henan, China). Glycerol (Analytical reagent) was obtained from Chengdu Kelon Chemical Reagent Plant (Sichuan, China). *E. coli* and *S. aureus* were obtained from Guangdong Microorganism Culture Collection Center (Guangdong, China). Distilled water was prepared in the laboratory.

2.2. Preparation of the films

The films were prepared following the process described as follows. First, the weighed nSA (0.15 %, w/v, the dosage was based on the preliminary experiment), TPs (0.05 %, w/v) and CS (2 %, w/v) were transferred to a beaker, and 2 % acetic acid and 1.5 % glycerin were added. The mixture was stirred at a constant rate, under a constant temperature water bath of 50 °C for 2 h. To check the effect of ultrasound on film forming properties, each solution was treated with different ultrasound in a TOPSONICS ultrasonic liquid processor (UP-400 series, Tehran, Iran), followed by vacuum pump treatment until the film-forming solution was bubble-free and uniform. Finally, the film-forming solution was poured onto a clean glass plate (250×150 mm) by casting method, dried in a 55 °C oven to form a dry film, and then peeled off and stored. All films were pretreated in an incubator at 25 °C and 50 % relative humidity for 24 h to keep them dry and then further tested. Table S1 shows the data of the different films prepared for this study. Fig. S1 shows the interaction mechanism of CS/nSA/TP composite films.

2.3. Single factor experiment

2.3.1. Effect of ultrasonication time on the performance of composite film

The stirred film liquid was placed into the ultrasonic wave for homogenization treatment, and the ultrasonic time was adjusted to 15 min, 30 min, 45 min and 60 min. The ultrasonic temperature was 30 °C, and the ultrasonic frequency was 40 kHz.

2.3.2. Effect of ultrasonication temperature on the performance of composite film

The stirred film liquid was placed into the ultrasonic wave for homogenization treatment, the ultrasonic temperature was changed to 10 °C, 20 °C, 30 °C, 40 °C, and 50 °C, the ultrasonic time was 30 min, and the ultrasonic frequency was 40 kHz.

2.3.3. Effect of ultrasonication frequency on the performance of composite film

The stirred film liquid was placed into the ultrasonic wave for homogenization treatment, the ultrasonic frequency was adjusted to 20 kHz, 25 kHz, 30 kHz, 35 kHz, and 40 kHz, the ultrasonic time was 30 min, and the ultrasonic temperature was 30 °C.

2.4. Physical properties

2.4.1. Mechanical properties

The tensile strength (TS) and elongation at break (EAB%) of the composite films were measured using a universal testing machine (HD-B609B-S, Haida Instrument, China). Before the test, the conditioned film was cut into 15×150 mm strips, and the thickness of film was measured. The initial gap of grip was 100 mm, and the speed of the mechanical crosshead to 50 mm/min. At least three replicates of each type of film were tested.

$$T_s = \frac{F}{S}E = \frac{L - L_0}{L} \times 100\% \quad (1)$$

T_s is the tensile strength (MPa); F is the maximum tensile force at which the specimen breaks (N); and S is the cross-sectional area of the specimen (mm^2). E is the elongation at break (%); L_0 is the original length of films (mm); and L is the length of the films breaking (mm).

2.4.2. Light transmittance

The film was cut into 10×40 mm splines, and each group made 6 parallel samples. An empty cuvette was used as a control to select a spline with a uniform thickness. The UV spectrophotometer (UV-2800, Unico Instrument, China) was preheated for 30 min, zero-adjusted, and adjusted to the natural light wavelength of 600 nm to conduct the light transmittance test [20]. The transmittance T of each group of films was measured. The average transmittance was calculated for each group.

2.4.3. Oil permeability coefficient

One milliliter of salad oil (rapeseed oil) was transferred to a test tube with an inner diameter of 13 mm. The test tube mouth was sealed with a film (50 mm × 50 mm) and inverted on the filter paper (20 mm × 20 mm) for 3 d under 50 % constant humidity. An electronic balance (JY3002, Hengping Science Instrument, China) was used to weigh the filter paper and calculate the oil permeability coefficient of the film according to the formula:

$$\Delta P_0 = \frac{\Delta M \times D}{S \times T} \times 100\% \quad (2)$$

Where ΔP_0 is the oil permeability coefficient ($\text{g mm/m}^2 \text{d}$); ΔM is the mass change of filter paper (g); D is the film thickness (mm); S is the film area (m^2); and T is time (d).

2.5. Response surface experiment

According to the single-factor experimental results, using ultrasonication time, temperature, and frequency as the test factors (Table S1), and the mechanical properties as the response value, three factors and three levels Box Behnken response surface methodology (RSM) were designed, in order to optimize the process. The response surface factors and levels are shown in Table 1. The optimum ratio of the three factors was obtained by process optimization. The mathematical regression model was established as:

$$Y = \beta_0 + \sum_{i=1}^3 \beta_{ij}X_i + \sum_{i=1}^2 \sum_{j=i+1}^3 \beta_{ij}X_iX_j + \sum_{i=1}^3 \beta_{ii}X_i^2 \quad (3)$$

where Y in the equation is the dependent variable, X_i and X_j were

Table 1
Response surface analysis factors and levels.

factors	levels		
	-1	0	1
Ultrasound time (X_1)/min	15	30	45
Ultrasonic temperature (X_2)/°C	20	30	40
Ultrasonic frequency (X_3)/kHz	30	35	40

independent variables of RSM, X_iX_j was interaction term of two factors, X_i^2 was quadratic term of independent variables for this experiment, β_0 , β_i , β_{ij} , β_{ii} were the regression coefficients for the intercept, linear, interaction, and quadratic, respectively.

2.6. Functional properties

2.6.1. Antioxidant property

The film was accurately weighed at 50 mg and sheared into powder, dissolved in 2 mL methanol, and soaked or stirred for 3 h by shaking. 0.5 mL sample solution was mixed with 2 mL 1,1-Diphenyl-2-trinitrophenylhydrazine (DPPH) ethanol solution with a concentration of 0.2 mmol/L, and the solution was reacted for 30 min in the dark environment. The absorbance value of the reaction solution was measured at 517 nm in a spectrophotometer (Ultraviolet-visible spectrophotometer, UV-2800, Shanghai, China). At the same time, the light absorption value of 0.5 mL methanol mixed with 2 mL DPPH ethanol solution for 30 min in the dark environment and 0.5 mL sample solution mixed with 2 mL ethanol were measured for comparison [9]. Each sample was measured in triplicate.

2.6.2. Antimicrobial activity

The antimicrobial properties of the films were determined using a modified version of the method described by Li et al. [21]. Gram-negative bacteria were represented by *E. coli* and gram-positive bacteria by *S. aureus*. Bacteria were cultured in a nutritive broth at 37 °C for 24 h to obtain 10^8 CFU/mL. The culture was then diluted to 10^6 CFU/mL, after which the films were sterilized under UV light for 1 h. Subsequently, 150 mg of sterilized films were mixed with 25 mL *E. coli* or *S. aureus* suspensions and placed in an oscillating water bath at 37 °C for 2 h to obtain the bacterial suspensions with films. Then, 0.1 mL of the *E. coli* or *S. aureus* suspension was diluted with sterile saline (0.85 % w/v), and 100 μL of this dilution was spread onto plate count agar plates. The plates were incubated at 37 °C with 75 % RH for 24 h, and the total number of colonies was recorded.

2.6.3. Indoor soil burial degradation

The soil was collected from the flower beds on campus, and the impurities were removed by hand. The soil was put into a 50 mL centrifuge tube. The composite film was cut into 2.5×2.5 cm small pieces, and the film samples were accurately weighed for recording. After that, the film samples were buried in the middle of the centrifuge tube, and the average values of soil temperature and relative humidity were 23 °C and 50 %. The degraded samples were taken out once a week and the soil on the film was removed with tweezers. The degraded samples were dried at room temperature for 1 h and weighed for four consecutive weeks.

2.7. Scanning electron microscopy and energy dispersive X-ray detector (SEM-EDX)

The dried composite film was cut into small sheets and ultrasonically dispersed in water. One drop of the dispersed droplet containing the sample was transferred to copper mesh and observed with a scanning electron microscope (S-3400 N, Hitachi Company, Japan) after the water volatilized. The EDX spectrometer equipped with SEM was used to analyze the elemental composition of nanoparticles under 10 kV acceleration voltage.

2.8. Transmission electron microscope (TEM)

20 mg sample was added into 3 mL ethanol, and the sample was dissolved in an ultrasonic bath. A drop of solution was taken from a 50 μL pipette and dropped onto the carrier film of copper mesh. After drying, the micro morphology of the nanocomposite film was observed by transmission electron microscope (S-3400 N, Hitachi Company,

Japan).

2.9. Fourier transform infrared spectroscopy (FTIR)

A film sample was transferred to a constant temperature drying oven at 50 °C for 12 h. Next, 1–2 mg of sample and 100–150 mg potassium bromide were completely ground and pressed it into a thin sheet in the mold. Infrared analysis was performed using a Fourier-transform infrared spectrometer (Billerica, MA, USA), with a scanning range of

4000–400 cm^{-1} , a resolution of 60, and a total of 32 scans.

2.10. Thermogravimetric analysis (DSC-TGA)

A thermogravimetric analyzer (Leco TGA 701; Leco, St Joseph, MI, USA), with a heating rate of 10 °C/min and temperature of 20–700 °C, was used to obtain the weight loss (TG) curve. The purge gas and shielding gas were both nitrogen, and the gas flow rate was 30 mL/min.

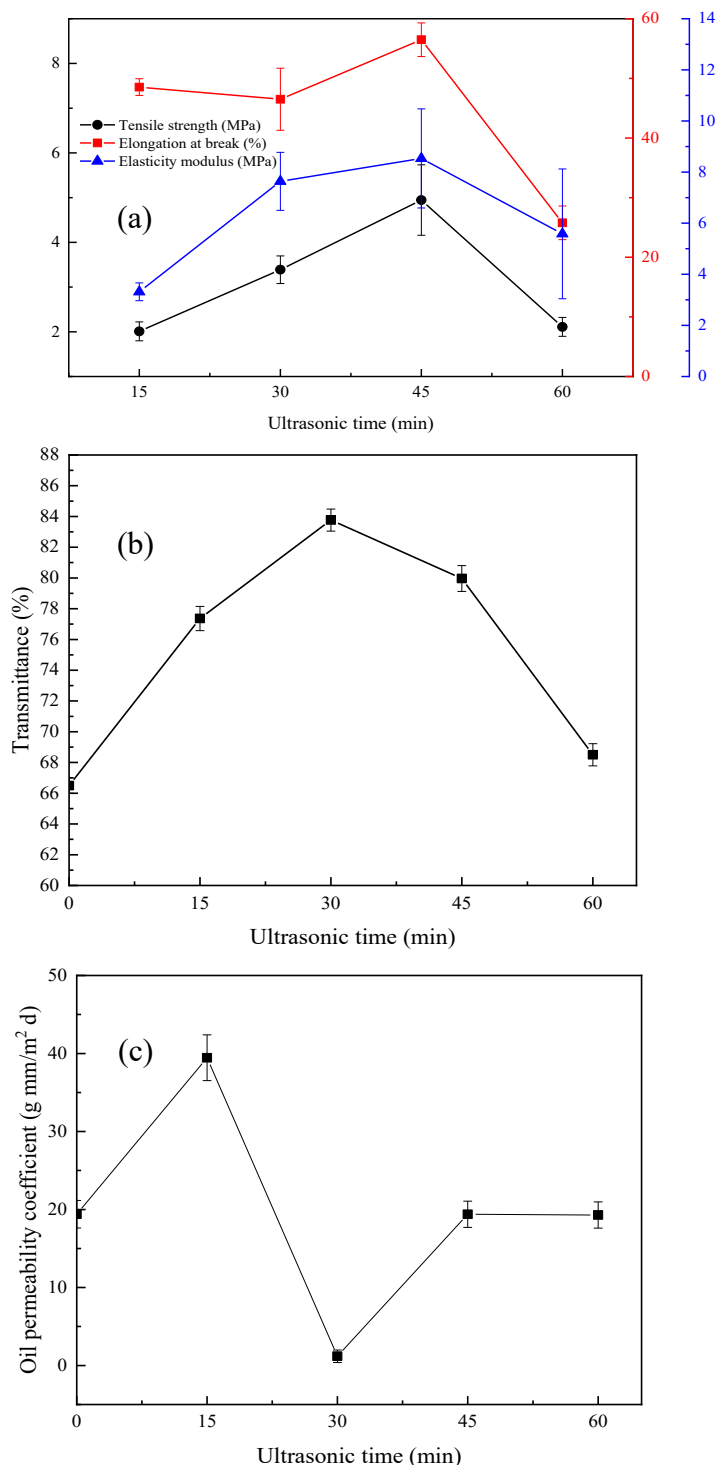


Fig. 1. The effect of ultrasonication time on the properties of the composite films. (a) Mechanical properties; (b) Light Transmittance; (c) Oil penetration coefficient.

2.11. Statistical analysis

The data obtained in this study were statistically analyzed by Microsoft Excel 2019, and plotted by Origin 2022. Statistical analysis was performed by IBM SPSS Statistics 22.0 digital software. Duncan method was used to verify the analysis of significant differences between groups. $p < 0.05$ means the difference is statistically significant, and the results are expressed as mean \pm standard deviation.

3. Results and discussion

3.1. The effect of ultrasonication time on the properties of the composite films

3.1.1. Mechanical properties

Elastic modulus (EM), tensile strength (TS), and elongation at break (EAB) can be used to describe the mechanical behavior of the sample because they are closely related to the internal structure of the sample. As shown in Fig. 1(a), the mechanical properties of the composite film have changed significantly ($p < 0.05$). As the duration of ultrasonic treatment increased, the TS, EAB, and EM gradually increased, reaching their respective maximums at 45 min. Its TS, EAB and EM were $(4.95 \text{ MPa} \pm 0.79) \text{ MPa}$, $(56.48 \pm 2.82) \%$ and $(8.53 \pm 1.94) \text{ MPa}$, respectively, indicating that the film is strong, flexible, and rigid. Borah et al. [22] also obtained a similar result. With the extension of ultrasonic processing duration, the super-mixing effect of the ultrasound rearranged the molecules to form a denser and more uniform network structure, thereby improving the mechanical properties of the composite films to some extent [13,23]. However, after this period of time had elapsed, the continuous increase in the duration of ultrasonic treatment led to a decrease in mechanical properties. The TS, EAB and EM of the films decreased from $(4.95 \text{ MPa} \pm 0.79) \text{ MPa}$, $(56.48 \pm 2.82) \%$ and $(8.53 \pm 1.94) \text{ MPa}$ to $(2.11 \pm 0.21) \text{ MPa}$, $(25.78 \pm 2.82) \%$ and $(5.58 \pm 2.54) \text{ MPa}$, respectively. Ultrasonic processing for an excessively long time, the mechanical properties of the films were decreased due to the increase of molecular motion and disorder of molecular alignment. Guo et al. [17] studied the effect of ultrasonication time on the properties of pectin films, and the results showed that van der Waals force could not maintain the adhesion between the film solution components during a longer ultrasonic processing time, thus forming a small cavity or microbubbles filled with gas. The growth of bubbles seemed to cause voids between molecules, thereby reducing the mechanical properties of the pectin films. Therefore, ultrasonic treatment can have a significant impact on the internal structure of the material and change its mechanical properties.

3.1.2. Light transmission

The light transmittance of the films greatly affects the appearance of the product [24]. The light transmittance of the polymer matrix is related to its internal structure, and the compact structure is not conducive to light transmission [25]. Yu et al. [26] showed that a wavelength of 600 nm can be used to measure the transparency of thin films. As shown in Fig. 1(b), the transmittance of the film is $(66.5 \pm 0.5) \%$ when the ultrasonication time is 0 min. With the prolongation of the ultrasonication time, the light transmittance of the films showed a trend of rising first and then falling. The light transmittance reached the highest value at $(83.77 \pm 0.72) \%$ after 30 min of ultrasonic treatment. Due to the short ultrasonication time, there may be aggregates/particles on the surface of the film, resulting in an increase in transmittance of the film. However, when the ultrasonication time was 45 min and 60 min, the transmittance of the film decreased by 4.75 % and 19.08 %, respectively. This may be due to the super-mixing effect of ultrasonication, resulting in a completely uniform distribution of TP molecules in the film-forming solution [27], thereby reducing the effect of ultrasonic treatment on light transmittance. Colodel et al. [28] reported similar results, in which the ultrasonication time was controlled to

produce films with appropriate characteristics, such as low light transmittance.

3.1.3. Oil penetration coefficient

In Fig. 1(c), ultrasonication time has a significant effect on the oil permeability of the composite films ($p < 0.05$). When the ultrasonication time was from 15 min to 30 min, the oil permeability of the films increased from $(19.40 \pm 1.77) \text{ g. mm/m}^2 \text{ d}$ to $(39.45 \pm 2.94) \text{ g. mm/m}^2 \text{ d}$ because the formation of small cavities that had not been eliminated destroyed the dense structure of the film. This is unfavorable for the films. When the ultrasonication time increased again, especially to 45 min, the oil permeability coefficient of the film was reduced by $39.34 \text{ g. mm/m}^2 \text{ d}$. According to Cruz-Diaz et al. [29], the tight structure of the film could provide greater mass transfer resistance, and the number of oil penetration paths through the polymer network would be limited. Because of the nSA network structure, the interaction between the polymer chains in the composite film could be enhanced. The intermolecular crosslinks were closer, and the compactness and continuity of the composite film were enhanced. At this time, the film had good barrier properties [30]. After 45 min of ultrasonication time, the oil permeability coefficient of the composite film increased again. The reason is that the longer the time, the more energy is absorbed, which breaks the hydrogen bonds between molecules of the film, consistent with the views of Suslick et al. [31].

3.2. The effect of ultrasonication temperature on the properties of the composite films

3.2.1. Mechanical properties

It can be seen from Fig. 2(a) that the ultrasonication temperature has a significant impact on the mechanical properties of the composite films ($p < 0.05$). When the ultrasonication temperature was from 10°C to 40°C , the TS and EM increased, and both reached the maximum at 40°C , with the maximum value of $(5.82 \pm 0.64) \text{ MPa}$ and $(68.57 \pm 22.13) \text{ MPa}$, respectively. The EAB reached the maximum value at 20°C , with the maximum value of $(195.15 \pm 18.50) \%$. At higher ultrasonication temperature, it was detrimental to the EAB of the film. The reason may be that with the increase of ultrasonication temperature, the intermolecular interactions are enhanced and the rigidity of polymer molecules increases, resulting in an increase in the TS and a decrease in the EAB of the film [29]. These observations were consistent with the results reported by Bae et al. [32]. When the ultrasonication temperature was further increased, the mechanical properties of the film gradually decreased. When the ultrasonic temperature exceeded 20°C , the EAB of the film rapidly decreased to $(46.5 \pm 5.2) \%$; when the ultrasonication temperature was 50°C , the TS and EM of the film were $(3.91 \pm 0.69) \text{ MPa}$ and $(33.95 \pm 1.47) \text{ MPa}$, respectively. It may be that the excessive ultrasonic temperature will destroy the structure of the film [33].

3.2.2. Light transmittance

From Fig. 2(b), with the increase of ultrasonic temperature, the light transmittance of the film first increased and then decreased. The transmittance of the film reached the highest value of $(83.77 \pm 0.72) \%$ when the ultrasonic temperature was 20°C . When the ultrasonic temperature was between 10°C and 20°C , the light transmittance of the film increased. Due to low temperature, the movement of TP particles was hindered, resulting in agglomeration of TP and other substances [34]. Therefore, the light transmittance of the composite film increased. With the continuous increase of ultrasonic temperature, the light transmittance coefficient of the composite film gradually decreased. When the ultrasonication temperature was 30°C and 40°C , the transmittance of the film was $(79.9 \pm 1.45) \%$ and $(79.5 \pm 1.19) \%$, respectively, without significant difference. When the ultrasonication temperature reached 50°C , the film transmittance further decreased to $(69.97 \pm 0.79) \%$. As the ultrasonic temperature increased, the movement of the material accelerated and the content was evenly dispersed.

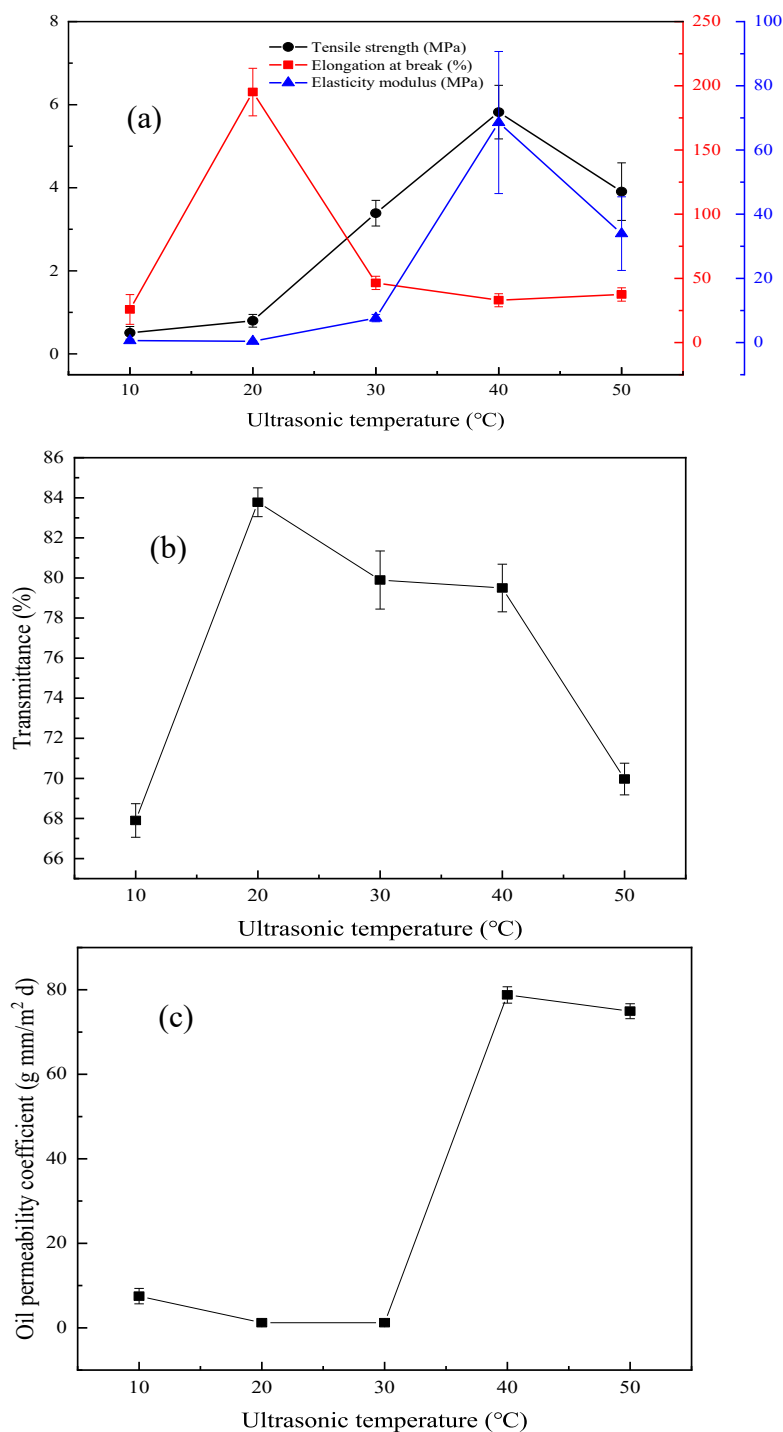


Fig. 2. The effect of ultrasonic temperature on the performance of composite film. (a) Mechanical properties; (b) Light Transmittance; (c) Oil penetration coefficient.

Therefore, once the aggregates were decomposed by ultrasound, more intermolecular interactions would occur, resulting in a stronger, more flexible, and tighter film [Ismael [35]]. The end result was a low light transmittance of the film.

3.2.3. Oil permeation coefficient

As can be seen from Fig. 2(c), ultrasonic temperature has a significant influence on the oil permeability coefficient of the film ($p < 0.05$). With the increase of ultrasonic temperature, the oil permeability of composite film generally presented a rising trend. When the ultrasonic temperature was 30 °C, the oil resistance of the composite film was the

best, which could reach (1.19 ± 0.17) g. mm/m² d. Because it had little effect on the dense network structure of the film at lower temperature, resulting in good oil resistance of the film. According to Del-Valle et al. [36], ultrasonic treatment at lower temperature has a significant effect on the supermixing of the film liquid of soybean protein isolate, resulting in a tighter structure of the film and enhanced oil resistance. When the temperature rose to 40 °C, the oil permeability coefficient of the composite film increased significantly to (78.78 ± 1.93) g. mm/m² d. This phenomenon may be caused by the cavitation effect of ultrasonic treatment. Ultrasonic treatment broke the original hydrogen bonds between CS and nSA, CS and TP molecules, reduced the intermolecular

force, and thus destroyed the tight structure between the molecules of the film, leading to the reduction of the barrier property of the film.

3.3. The effect of ultrasonication frequency on the performance of the composite films

3.3.1. Mechanical properties

High-intensity ultrasound usually uses a lower frequency in the range of 20–100 kHz, and its application in the food industry is

relatively new. Under high-intensity conditions, ultrasound can generate a strong pressure shear and temperature gradient inside the material, thereby physically destroying its structure, or promoting certain chemical reactions. Low-frequency high-power ultrasound has enough energy to break intermolecular bonds [37]. As can be seen from Fig. 3(a), ultrasonic frequency has a significant impact on the mechanical properties of composite films ($p < 0.05$). At the beginning, the rupture of large aggregates was caused by the propagation of high-intensity ultrasound, which resulted in an overall increase in the TS,

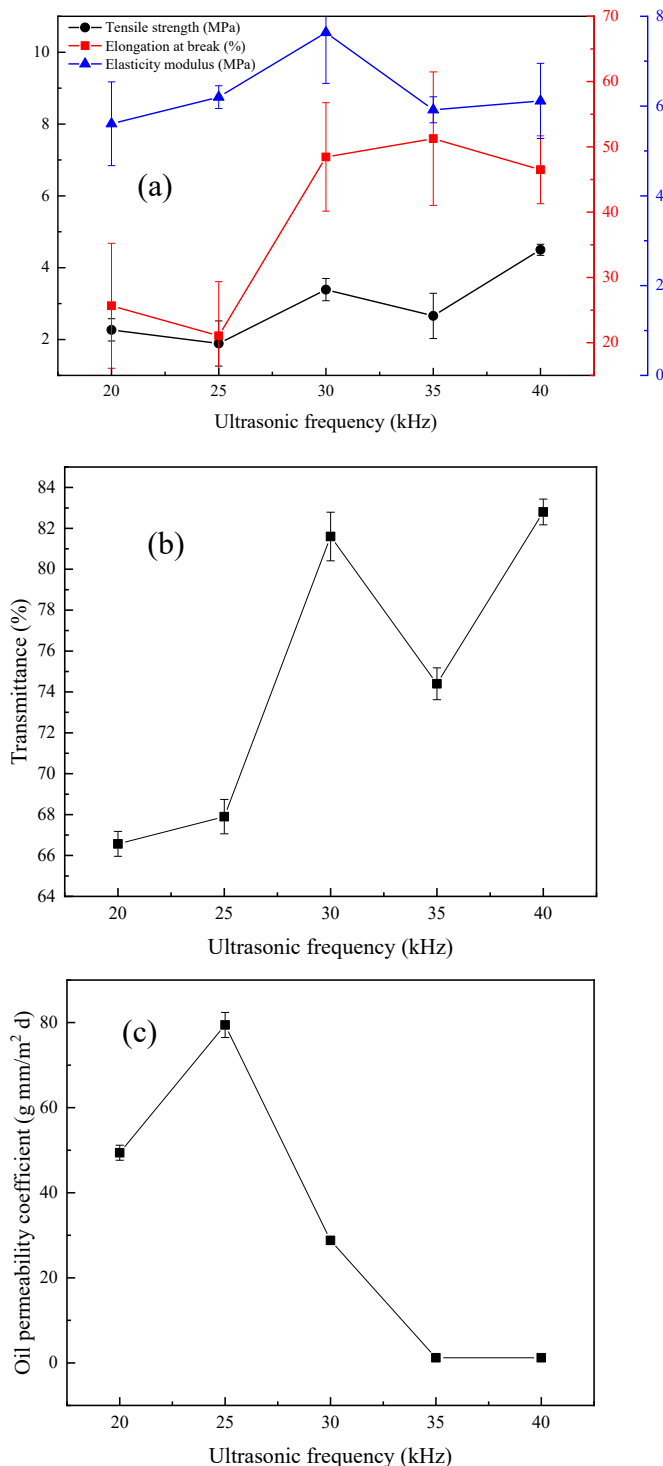


Fig. 3. The effect of ultrasonic frequency on the performance of composite film. (a) Mechanical properties; (b) Light Transmittance; (c) Oil penetration coefficient.

EAB and EM of the films. This finding could be because ultrasound was stronger than mechanical agitation. Therefore, cavitation effects led to uniform distribution of particles at the microscopic level, conducive to molecular interactions [38]. When the ultrasonic frequency was 30 kHz, the film had good mechanical properties, its TS, EAB and EM reached (3.39 ± 0.31) MPa, (48.46 ± 8.3) % and (7.64 ± 1.13) MPa, respectively. It was worth noting that as the ultrasonic frequency continued to rise, the TS and EM of the films decreased, while the EAB obtained at 30 kHz was not significantly different from that at 40 kHz. This phenomenon could be called “overprocessing effect”.

3.3.2. Light transmission

When the ultrasonic frequency increased, the transmittance of the composite films showed an overall increasing trend (Fig. 3(b)). When the ultrasonic frequency increased from 20 kHz to 30 kHz, the transmission coefficient increased by 22.39 %. Similarly, Brodnjak [39] improved the optical properties of chitosan/rice starch films by ultrasound. This was because the fine particles in the film-forming liquid moved and separated under the action of ultrasonic wave. The minimization of intermolecular forces led to the gradual breaking of chemical bonds, resulting in the increase of light transmittance of the composite film. In addition, glycerin had been reported to affect the color of the film [39]. Due to small steric hindrance, glycerol was easily embedded between macromolecules in the film, resulting in a decrease in the tightness of the film. The color of the film becomes lighter, enhancing the transmittance of composite film. When the ultrasonic frequency was 30 kHz and 40 kHz respectively, the transmittance of the film was not different. Therefore, when the ultrasonic frequency was 30 kHz, the film had good light transmittance.

3.3.3. Oil penetration coefficient

From Fig. 3(c), the ultrasonic frequency has a significant effect on the oil permeability of the composite films ($p < 0.05$), and the overall trend is that it first increases and then decreases. The factors that affected the size of the oil permeability coefficient were mainly related to the lipophilic groups contained in the composite film [40] and the compact structure of the film. When the ultrasonication frequency was 25 kHz, the maximum oil permeability coefficient of the film was (79.45 ± 2.94) g. mm/m² d, indicating that the oil resistance of the film was very poor at this time. The reason may be that the nSA itself is a hydrophobic substance. When the ultrasonication frequency was low, its power was higher, which could cause the lipophilic group in the film to be exposed [41]. It might also make the structure of the film less compact, resulting in an increase in the oil permeability of the film. When the ultrasonication frequency continued to increase, hydrophilic substances, such as CS and glycerin, would be more uniformly dispersed. This led to the enhanced performance of the composite film to prevent oil penetration. The data showed that when the ultrasonication frequency was 35 kHz and 40 kHz, the oil permeability coefficient of the film was the best, which were (1.19 ± 0.8) g. mm/m² d and (1.20 ± 0.68) g. mm/m² d, respectively.

3.4. Response surface experiment results

3.4.1. Experimental design results

Using single factor test results, ultrasonication time (min), temperature (°C), and frequency (kHz) were selected as independent variables, and the mechanical properties of the film were the response values. The response surface analysis of three factors and three levels was carried out by Design Expert 8.0.6 software, and the experimental combination and results obtained were shown in Table S2.

Design Expert 8.0.6 software was used to establish the relationship between the influencing factors and the performance of the CS/nSA/TP composite film. The regression equations of performance, as well as ultrasonication time, temperature, and frequency, were obtained. Finally, regression analysis was performed on the data with SPSS22

software. The results are shown in Table 2. The F values of tensile strength and elongation were 21.51 and 7.32, respectively, indicating that the model was statistically significant. The goodness of the model can be tested by determinant coefficient (R^2). The coefficient of determination ($R^2 = 90.40$ %) calculated by the quadratic regression model showed that only 9.60 % of the total change could not be explained by the model, indicating that the model was reasonable to fit the experimental data.

3.4.2. Analysis of interactive impact of response surface

The interactive effects of the three factors on the performance of the composite films are shown in Fig. 4. The steeper the slope of the response surface, the more sensitive the performance of the composite film is to the variable of the two factors. Conversely, the smoother the surface, the weaker the interaction. The response surface model diagram intuitively reflects the impact of the three ultrasonication processes on the performance of the composite film [42]. The ultrasonic treatment modified the mechanical properties of the films, which became more resistant to mechanical stress and more flexible. Increased molecular interactions due to energy input might result in higher molecular order, thus increasing the film strength. The analysis of the response surface diagram of the interactive impact of the ultrasonication process on the tensile strength shows that the ultrasonication frequency has a weaker effect on the tensile strength of the composite film. The ultrasonication temperature and time have greater impacts on the tensile properties of the composite film. For the analysis of the elongation interaction of the composite film, the ultrasonication time and frequency had less dramatic effects on the elongation. The contour map shows that the two factors are in a non-obvious elliptical shape. Therefore, the significance of the interaction of the two factors is low [43]. The prediction value was estimated and predicted by software. The best ultrasonication conditions for predicting the tensile strength of the composite film are: ultrasonication time (57.97 min), temperature (37.26 °C) and frequency (30 kHz). In addition, the maximum tensile strength reached 4.036 MPa. The best ultrasonication conditions for predicting the elongation of the composite film are: the ultrasonication time (60.88 min), temperature (39.93 °C) and frequency (30 kHz). The maximum elongation reached 279.42 %.

3.5. Antioxidant performance

The properties of the films were improved by proper ultrasonic treatment of the film-forming solution. According to the above results, CS/nSA/TP composite films were considered to have the best mechanical properties and good light transmittance and barrier performance at ultrasonication time (57 min), temperature (37 °C) and frequency (30 kHz). Therefore, this type of film (CS/nSA/TP(+)) was selected for antioxidant, antibacterial and degradation tests. Moreover, CS, CS/nSA, CS/TP and CS/nSA/TP(+) films were prepared under the same conditions, where CS/nSA/TP(-) was a film without ultrasonic treatment.

DPPH radicals are widely used to determine the free radical scavenging ability of compounds and thus to evaluate the antioxidant

Table 2

Regression equation of the influence of ultrasonic time, ultrasonic temperature, and ultrasonic frequency on the performance of composite film.

Variable	Fitting equation	F value	Standard deviation	R ²
Tensile Strength	$2.66 + 1.20X_1 + 1.57X_2 + 0.47X_3 - 0.15X_1X_2 - 0.023X_1X_3 + 0.49X_2X_3 + 0.43X_1^2 - 0.047X_2^2 + 0.21X_3^2$	21.51	0.43 MPa	0.9651
Elongation	$1.62 - 0.03X_1 - 0.016X_2 - 0.03X_3 + 0.055X_1X_2 - 0.042X_1X_3 + 0.09X_2X_3 - 0.40X_1^2 - 0.22X_2^2 - 0.58X_3^2$	7.32	0.20 %	0.9040

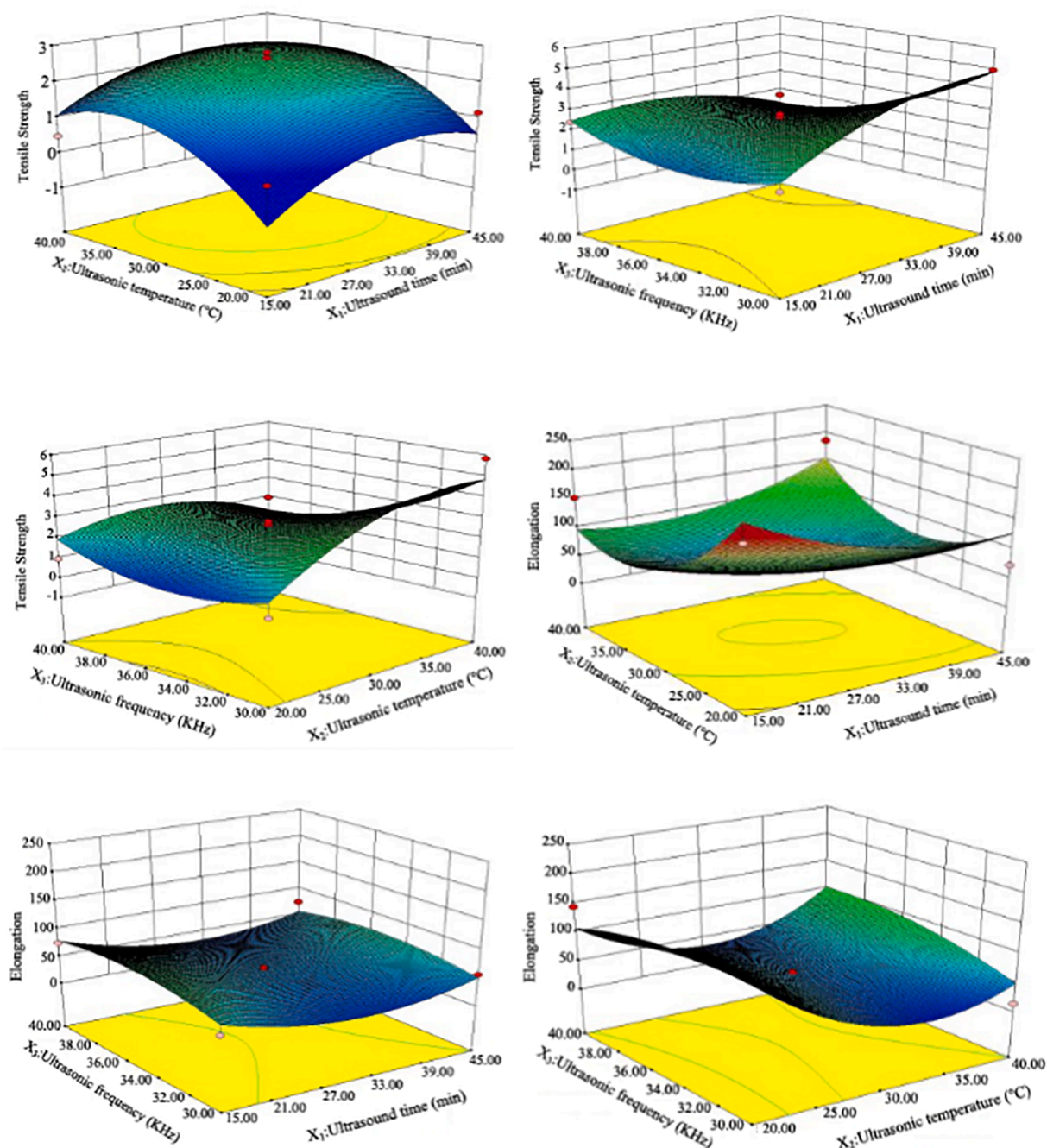


Fig. 4. Response surface diagram of the effect of the interaction of ultrasonic time, ultrasonic temperature, and ultrasonic frequency on the mechanical properties of composite films.

activity of such substances. Fig. 5(a) shows the change of free radical scavenging ability of different composite films. The DPPH scavenging capacity of the pure CS film and CS/nSA film was $(10.20 \pm 1.73) \%$ and $(14.09 \pm 1.31) \%$, respectively, with no significant difference, which was similar to previous studies [44]. After adding TP, the free radical scavenging ability of the film was significantly improved. The antioxidant principle of TP was to terminate the free radical chain reaction and use phenolic hydroxyl groups with strong hydrogen supply capacity to remove reactive oxygen species. This result was consistent with that of Wang et al [45]. They also observed that when TP content was too high, a large number of TP molecules formed a granular layer on the surface of the nanocomposite film, which gradually consumed phenolic hydroxyl by oxygen in the air, resulting in a decrease in the increase of DPPH free radical clearance rate. In this experiment, the mass ratio of CS, nSA and

TP was fixed, and the oxidation resistance of the film could be further improved by changing the ultrasonic conditions. The DPPH radical scavenging rates of CS/TP, CS/nSA/TP(-) and CS/nSA/TP(+) films were $(44.06 \pm 2.54) \%$, $(47.89 \pm 1.16) \%$ and $(52.58 \pm 1.64) \%$, respectively. The radical scavenging ability of CS/nSA/TP(-) film was slightly higher than that of CS/TP film, which may be due to the weaker oxidation resistance of nSA itself. The more critical information is that compared with CS/nSA/TP(-) film without ultrasonic treatment, CS/nSA/TP(+) film significantly improved the free radical scavenging rate. This may be because more TP particles are protected by the three-dimensional network structure composed of CS and nSA after ultrasonic treatment [45]. Cuevas-acuna et al. [46] also found that short time and high amplitude high-intensity ultrasonication treatment could improve the free radical scavenging ability of chitosan-gelatin film. Here, the high

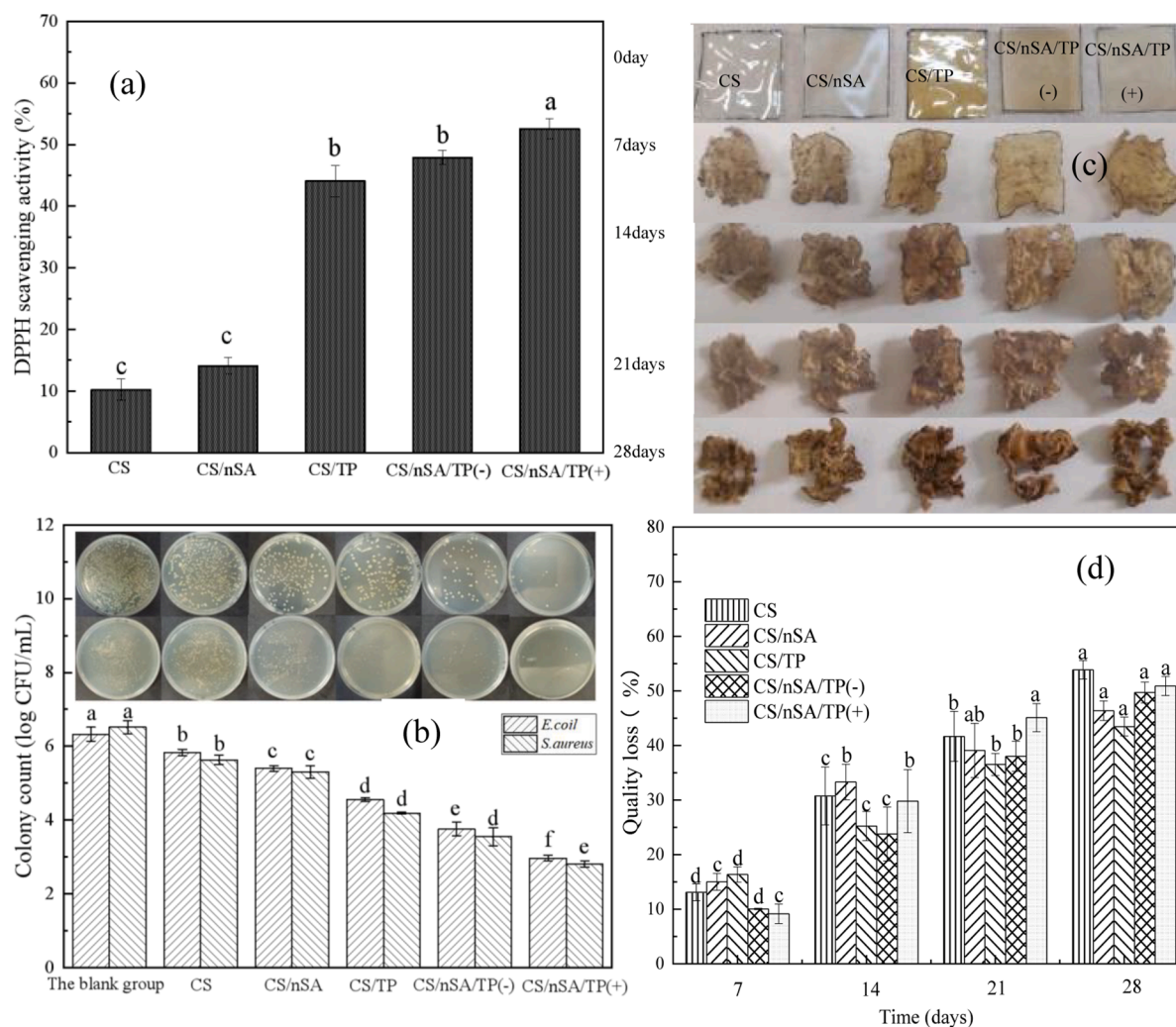


Fig. 5. Effect of ultrasonic treatment on functional properties of the composite films. (a): DPPH radical scavenging activity. (b): Growth of *E. coli* and *S. aureus* in different film solutions. (c)-(d): The visual image and quality loss of CS, CS/nSA, CS/TP, CS/nSA/TP(-) and CS/nSA/TP(+) films after being buried in soil from day 0 to 28 days.

DPPH free radical scavenging activity was mainly based on the synergistic effect of TP and CS.

3.6. Antimicrobial activity

Microorganisms are an important cause of food spoilage. Therefore, evaluation of antibacterial performance is very important for food packaging [47]. The antibacterial activities of different CS-based films against Gram-negative (*E. coli*) and Gram-positive (*S. aureus*) were shown in Fig. 5(b). When CS was added to the blank group, the number of viable *E. coli* decreased from (6.33 ± 0.19) log CFU/mL to (5.83 ± 0.09) log CFU/mL, and the number of viable *S. aureus* decreased from (6.52 ± 0.18) log CFU/mL to (5.63 ± 0.13) log CFU/mL. This indicates that CS had a significant bacteriostatic effect on both *E. coli* and *S. aureus*, however the relative inhibitory effect of CS on *S. aureus* was more significant ($p < 0.05$). These findings were consistent with literature reports [48]. It has been reported that the properties of bacterial surface membranes were altered and destroyed due to electrostatic interactions between positively charged CS molecules and negatively charged bacterial membranes [49]. The results showed that the addition of nSA and TP could improve the inhibitory effect of CS on bacteria, but TP played a major role. The mechanism of adding nSA to enhance the antibacterial ability may be that nSA not only increases its contact with the bacterial membrane, but may also interacts with the protein on the

bacterial surface [50]. TPs mainly lead to cell division and metabolic disorder by changing cell morphology. It is worth noting that in the film, CS, nSA and TP may have a certain synergistic effect on the antibacterial activity. In addition, similar synergistic effects have also been found in other nanomaterials such as TiO_2 and ZnO [51].

Studies showed that CS/nSA/TP(-) and CS/nSA/TP(+) films had the best antibacterial activity. The number of viable *E. coli* was (3.76 ± 0.18) log CFU/mL and (2.97 ± 0.07) log CFU/mL, respectively, while the number of viable *S. aureus* was (3.55 ± 0.24) log CFU/mL and (2.81 ± 0.08) log CFU/mL, respectively. These observations showed ultrasonic treatment could improve the bacteriostatic effect of the material to a certain extent [13]. This may be because the TP particles in the film solution treated by ultrasonic were better protected by the 3D network structure composed of CS and nSA. Therefore, the enhancement effect of ultrasonic treatment on the antibacterial properties of the films deserves further study.

3.7. Biodegradability analysis

Fig. 5(c and d) shows the visual image and quality loss of CS, CS/nSA, CS/TP, CS/nSA/TP(-) and CS/nSA/TP(+) films buried in the soil every 7 days. Overall, degradation of CS-based films in soil was first observed by the naked eye. The films lost their original appearance and structural integrity, and the surface appeared rough and eroded surfaces, with

porous pits and holes. On day 7, all films were wrinkled, especially the CS film was broken and partially degraded (the missing part on both sides and the central hole), indicating that the microbial presence in the soil had a high degree of biodegradation of the film [52]. With the increase of days, the cross-linking between film components was

destroyed, resulting in increased degradation. Due to the use of CS as a carbon and nitrogen source for metabolic growth of soil microorganisms, the surface roughness of the film increased after the samples were exposed to soil microorganisms, resulting in pits, erosion areas and cracks [53]. This process of soil biodegradation might lead to surface

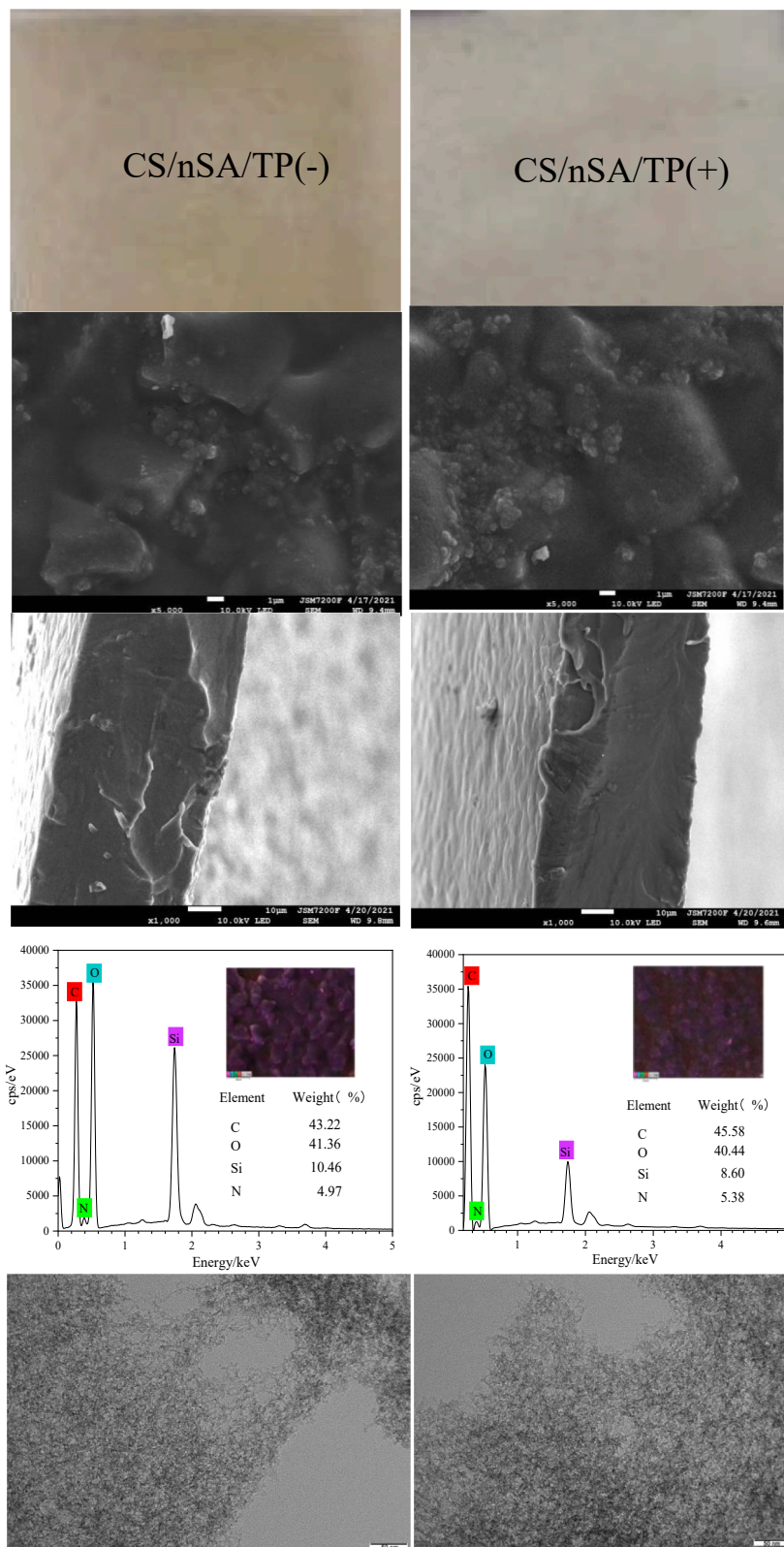


Fig. 6. Photographs, SEM images, EDX spectra and TEM images of the films.

corrosion, because pitting and degradation of surface materials might further penetrate into the interior of the film [54].

The quantitative index of biodegradability of films was estimated by weight loss method. It is obvious that the degradation rate of CS film increased rapidly with an almost constant gradient every 7 days. The degradation rates were $(13.09 \pm 1.55) \%$, $(30.74 \pm 5.30) \%$, $(41.66 \pm 4.58) \%$ and $(53.84 \pm 1.70) \%$, respectively. It was indicated that CS-based film was a promising biodegradable film. However, when nSA was added to CS, the film degradation rates were $(15.00 \pm 1.55) \%$, $(33.30 \pm 3.26) \%$, $(39.08 \pm 4.97) \%$ and $(46.36 \pm 1.78) \%$, respectively, every 7 days. These observations indicate that the addition of nSA can reduce the degradation of the film. The same results were seen for CS/TP film. This phenomenon may be caused by the formation of the 3D network structure composed of CS and nSA (or TP), which slows down the degradation of the film. It was worth noting that within 7 days, the degradation rate of CS/nSA/TP(-) film was higher than that of CS/nSA/TP(+) film, and then the degradation rate of CS/nSA/TP(-) film was lower than that of CS/nSA/TP(+) film. It showed that the ultrasonic technology had a certain influence on the degradation rate of film. Ultrasonic processing may have increased the degradation rate of the composite film on account of the cavitation and super-mixing effects, which conferred a smoother surface, making the film more prone to degradation. Deshmukh et al. [54] showed that the CS/DCB composite film had a degradation rate of more than 50 % in a 60-day soil burial test. Oberlinter et al. [55] also reported that the active chitosan biopolymer film rich in quercetin polyphenol extract was biodegradable in soil after 14 days. Therefore, the CS/nSA/TP composite film can be considered as a biodegradable film due to its rapid degradation process.

3.8. Structural characterization

3.8.1. SEM-EDX and TEM analysis of film

Fig. 6 shows photographs, SEM images, EDX spectra and TEM images of the films. All films had a continuous and smooth appearance, indicating good compatibility between the components of the matrix. In contrast, CS/nSA/TP (+) films appeared pale yellow, which might be due to the uniform distribution of TP particles in the three-dimensional structure of CS and nSA by ultrasonic action.

The morphology of the thin films was characterized by scanning electron microscopy. Untreated films have a thicker cross section. In contrast, the films treated by ultrasound were more uniform and had less surface agglomeration. This difference in structure can be attributed to the interaction between CS and nSA and ultrasonic cavitation to form a tighter structure of the film [56]. In order to determine the element composition of CS matrix composite films and the good distribution of nSA, element mapping was carried out related to EDX spectral analysis. In Fig. 6, the uniform distribution of nSA in CS matrix was observed. In addition, compared with CS/nSA/TP(-) film, the increase in the content of C and O elements is due to the increase in the number of hydrogen bonds formed between the film forming materials after ultrasonic treatment. However, the relative content of Si decreased, which might be due to the fact that nSA particle content became difficult to detect because the particles are better distributed in the polymer matrix. This result confirmed that, as reported by Cabello-Alvarado et al. [57] ultrasonic treated TiO₂ facilitated dispersion in thermoplastic materials. It was further found by TEM that nSA in CS/nSA/TP(+) films had many pores with approximate pore sizes ranging from 5 nm to 100 nm. Ultrasound made nSA dispersion more uniform [58].

Fig. 7 shows the SEM of the composite films with different ultrasonic time, frequency and temperature. As the ultrasound time increased, the pores inside the film decreased in size, the component distribution became more uniform, and the particle agglomeration phenomenon improved. This was a good indicator of better structure and mechanical properties [39]. The change in ultrasonication temperature had no significant effect on the surface morphology of the film, but the surface of the film was smoothest when the temperature was 20 °C. At 40 °C, there

were many agglomerated particles in the cross section of the film. When the ultrasonication frequency was 35 kHz, many nSA agglomerates appeared on the surface of the film. Conversely, when the frequency was 30 kHz and 45 kHz, the agglomeration phenomenon reduced, indicating that the appropriate frequency can inhibit the agglomeration of nSA particles and increase its dispersion. This is consistent with our assumptions, when analyzing the mechanical properties of the films.

3.8.2. FTIR analysis of film

In order to further analyze the molecular interaction of CS/nSA/TP films, Fourier transform infrared spectroscopy (FTIR) of the film was studied. As shown in Fig. 8a and b, the broad band between 3600 and 3000 cm⁻¹ is the association structure of -OH in CS and nSA [59], the stretching vibration of O-H on the side group of CS, and the asymmetric and symmetric stretching vibrations of N-H [60,61]. After the addition of nSA and TP, some changes occurred in the band position and strength of the chitosan-based film. More specifically, The O-H and N-H stretching vibration absorption peaks of chitosan based films moved to lower wave number (blue shift) compared with CS film. Such observation indicated that there was no chemical interaction but physical intermolecular interaction. The band indicates that there was hydrogen bonding after the reaction [62]. The absorption peak at 1600–1500 cm⁻¹ was caused by the stretching vibration of -C=O- in the CS structure, N-H bending [63], and the asymmetry of Si-OH in nSA [64]. The absorption peak at 1500–1000 cm⁻¹ was attributed to C-H bending vibration, O-H deformation [65] and C-O stretching of primary alcohol groups [66]. The absorption peak around 1040 cm⁻¹ corresponded to the stretching motion of C-O-C in the structure. The band at 886 cm⁻¹ was also caused by the polysaccharide structure of CS. Compared with the non-ultrasonic film, the spectrum of ultrasonic treatment film was significantly blue shifted at 1600–1100 cm⁻¹ absorption peak, and the intensity of the absorption peak at 1590 cm⁻¹ was much higher than that of the ultrasonic film at 1640 cm⁻¹. This phenomenon indicated that the components in the ultrasound-treated film were more tightly bound and more evenly dispersed. As shown in Fig. 8(b), as the ultrasound time (15 min, 30 min, 45 min), ultrasound temperature (20 °C, 30 °C, and 40 °C) and ultrasound frequency (30 kHz, 35 kHz, and 40 kHz) increased, the composite film did not significantly change. Moreover, the molecular structure was not significantly damaged. Under different ultrasonication time, temperature, and frequency, the three components of CS/nSA/TP composite film maintain good compatibility.

3.8.3. Thermogravimetric analysis (TGA) of films

According to the change of molecular structure in packaging material with temperature, the characteristic parameters of thermostable film TG-DTG curve were analyzed, as shown in Table S3. TG-DTG curve of the film was shown in Fig. 8(c). TGA results of different ultrasonic treatments showed that the weight loss in the film could be divided into two stages, T_s, T_d, T_p and T_e represented the starting, decomposition, peak and end temperatures of the film respectively. As can be seen from Fig. 8, CS/nSA/TP(-) film had the largest weight loss rate, and the final mass residue of the film was 26.8 %, while the remaining mass residue was more than 33 %. This was because the interaction between the polymer chains was enhanced after ultrasonic treatment, which made the network in the film denser and tighter, leading to ultrasonic treatment could improve the thermal stability of the film. There was a small amount of weight loss (about 13 %) in the first decomposition stage (T_s-T_d). The slight weight loss below 100 °C was due to evaporation of water and volatilization of small molecules such as glycerol in the film [67]. The weight loss mainly occurred in T_d-T_e, and the maximum decomposition rate occurred around 300 °C. At this stage, the total mass loss rate was about 50 % due to the decomposition of the polymer backbone [68]. In addition, the loss of adjacent hydroxyl groups and the rupture of glycosidic bonds might also occur [24]. When the ultrasonic frequency was 30 kHz, 35 kHz and 40 kHz, T_d was 223.0 °C, 224.4 °C and 231.1 °C,

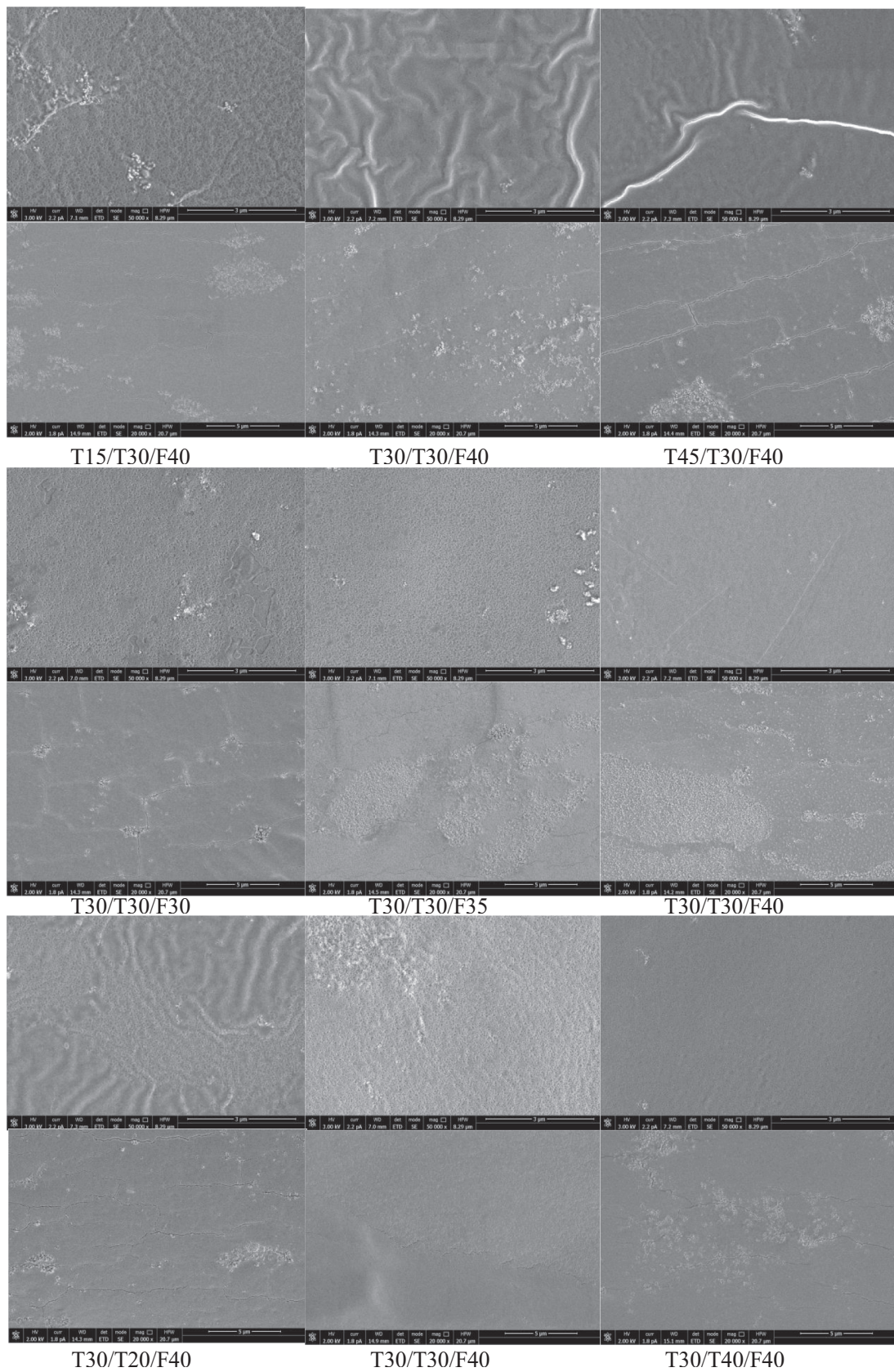


Fig. 7. Effect of ultrasonic time, frequency, and temperature on SEM of CS/nSA/TP films.

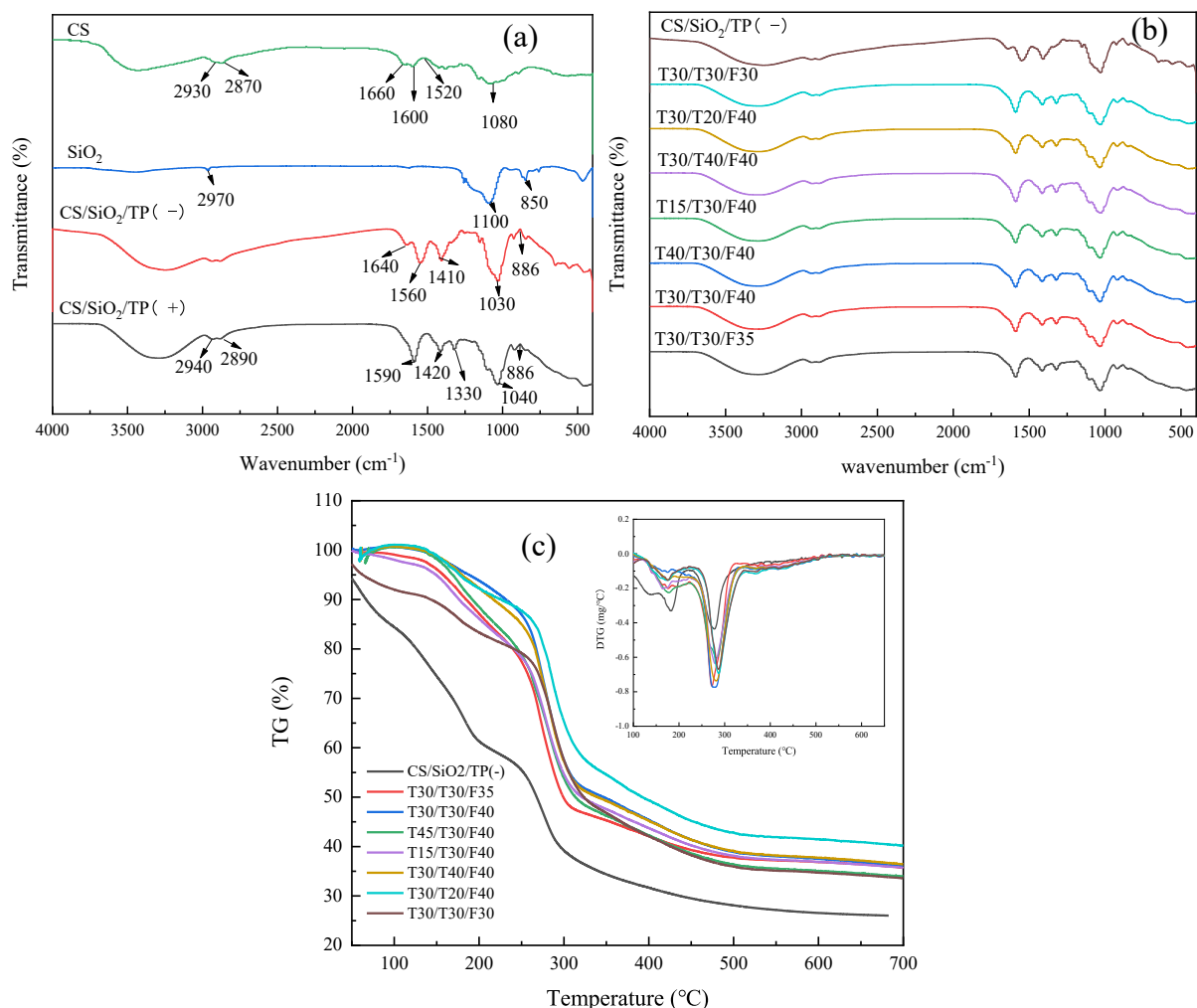


Fig. 8. FTIR analysis and TG-DTG curves of composite films.

respectively. Increasing the frequency can improve the thermal stability of the film, which may be related to the uniform distribution of nSA in the film. The strong interaction between CS molecules and Si-OH in nSA delayed the movement of molecular chain, thus enhancing the thermal stability of the film. With the increase of ultrasonic temperature, T_d of the film decreased because the chemical bond between the film forming material molecules and water/glycerol was destroyed when the temperature increased [17]. When the ultrasonic time was 15 min, 30 min and 45 min, T_s was 46.8 °C, 51.4 °C and 79.7 °C, respectively. Therefore, increasing ultrasonic time could improve the thermal performance of the film. After prolonged ultrasonication time, the film-forming material molecules formed many chemical bonds with water and glycerol molecules [69], which prevented the diffusion of water and glycerol molecules, leading to the increase of T_s . The above results showed that ultrasonic treatment inhibited the thermal decomposition of the film and improved the thermal stability of the film. Similar results have been reported for polysaccharide based films [68]. Therefore, the thermal stability of the composite films can be improved by appropriate ultrasonic treatment.

4. Conclusion

In this study, we successfully prepared CS/nSA/TP composite films, and used ultrasound to improve the quality of the film. The prepared films had good oil resistance and light transmittance. The best

conditions for mechanical properties were ultrasonic time of 57 min, ultrasonic temperature of 37 °C, and ultrasonic frequency of 30 kHz. The experiment also verified the previous hypothesis that the addition of TP improved the oxidation resistance of the film, and the oxidation resistance of the film was further improved by ultrasonic treatment. The film had strong antibacterial activity against *E. coli* and *S. aureus*. Buried in soil after 28 d, the biodegradation rate of the film was 50.88 %. Ultrasonic treatment promoted the formation of hydrogen bonds among film-forming materials and improved the thermal stability of the composite films. These data indicate that ultrasonic treatment provides a simple and green method to improve the performance of the film and broaden its application.

Declaration of Competing Interest

The authors declare that they have no known competing financial interests or personal relationships that could have appeared to influence the work reported in this paper.

Acknowledgements

The author thanks 211 Engineering Double Support Plan (No. 2121993039) for financial support.

Appendix A. Supplementary data

Supplementary data to this article can be found online at <https://doi.org/10.1016/j.ultsonch.2022.106052>.

References

- [1] M. Dash, F. Chiellini, R.M. Ottenbrite, E. Chiellini, Chitosan-A versatile semi-synthetic polymer in biomedical applications, *Prog. Polym. Sci.* 36 (8) (2011) 981–1014.
- [2] C.L.O. Petkowicz, P.A. Williams, Pectins from food waste: characterization and functional properties of a pectin extracted from broccoli stalk, *Food Hydrocolloids* 107 (2020) 105930.
- [3] S. Kumar, A. Mukherjee, J. Dutta, Chitosan based nanocomposite films and coatings: emerging antimicrobial food packaging alternatives, *Trends Food Sci. Technol.* 97 (2020) 196–209.
- [4] M. Aider, Chitosan application for active bio-based films production and potential in the food industry: review, *Lwt-Food Sci. Technol.* 43 (6) (2010) 837–842.
- [5] N.E. Kochkina, N.D. Lukin, Structure and properties of biodegradable maize starch/chitosan composite films as affected by PVA additions, *Int. J. Biol. Macromol.* 157 (2020) 377–384.
- [6] M. Ji, J. Li, F. Li, X. Wang, J. Man, J. Li, C. Zhang, S. Peng, A biodegradable chitosan-based composite film reinforced by ramie fibre and lignin for food packaging, *Carbohydr. Polym.* 281 (2022) 119078.
- [7] Q. Zeng, T. Mao, H.D. Li, Y. Peng, Thermally insulating lightweight cement-based composites incorporating glass beads and nano-silica aerogels for sustainably energy-saving buildings, *Energy Build.* 174 (2018) 97–110.
- [8] A. Aragon-Gutierrez, M.P. Arrieta, M. Lopez-Gonzalez, M. Fernandez-Garcia, D. Lopez, Hybrid biocomposites based on poly(lactic acid) and silica aerogel for food packaging applications, *Materials* 13 (21) (2020) 4910.
- [9] D. Lin, Y. Zheng, Y. Huang, L. Ni, J. Zhao, C. Huang, X. Chen, X. Chen, Z. Wu, A.M. Osman, Q. Zhang, W. Qin, B. Xing, Investigation of the structural, physical properties, antioxidant, and antimicrobial activity of chitosan-nano-silicon aerogel composite edible films incorporated with okara powder, *Carbohydr. Polym.* 250 (2020) 116842.
- [10] L.Y. Wang, Y. Dong, H.T. Men, J. Tong, J. Zhou, Preparation and characterization of active films based on chitosan incorporated tea polyphenols, *Food Hydrocolloids* 32 (1) (2013) 35–41.
- [11] M. Afzal, A.M. Safer, M. Menon, Green tea polyphenols and their potential role in health and disease, *Inflammopharmacology* 23 (4) (2015) 151–161.
- [12] A.M. Osman, Multiple pathways of the reaction of 2,2-diphenyl-1-picrylhydrazyl radical (DPPH center dot) with (+)-catechin: evidence for the formation of a covalent adduct between DPPH center dot and the oxidized form of the polyphenol, *Biochem. Biophys. Res. Commun.* 412 (3) (2011) 473–478.
- [13] Y.W. Liu, S.Y. Wang, W.J. Lan, W. Qin, Development of ultrasound treated polyvinyl alcohol/tea polyphenol composite films and their physicochemical properties, *Ultrason. Sonochem.* 51 (2019) 386–394.
- [14] J. Liu, S. Liu, Q.Q. Wu, Y.Y. Gu, J. Kan, C.H. Jin, Effect of protocatechuic acid incorporation on the physical, mechanical, structural and antioxidant properties of chitosan film, *Food Hydrocolloids* 73 (2017) 90–100.
- [15] W.L. Zhang, W.B. Jiang, Antioxidant and antibacterial chitosan film with tea polyphenols-mediated green synthesis silver nanoparticle via a novel one-pot method, *Int. J. Biol. Macromol.* 155 (2020) 1252–1261.
- [16] L. Wang, J. Ding, Y. Fang, X. Pan, F. Fan, P. Li, Q. Hu, Effect of ultrasonic power on properties of edible composite films based on rice protein hydrolysates and chitosan, *Ultrason. Sonochem.* 65 (2020).
- [17] Z.L. Guo, X.Z. Ge, L.H. Yang, Q.M. Gou, L. Han, Q.L. Yu, Utilization of watermelon peel as a pectin source and the effect of ultrasound treatment on pectin film properties, *Lwt-Food Sci. Technol.* 147 (16) (2021) 111569.
- [18] P. Liu, W. Gao, X. Zhang, B. Wang, F. Zou, B. Yu, L. Lu, Y. Fang, Z. Wu, C. Yuan, B. O. Cui, Effects of ultrasonication on the properties of maize starch/stearic acid/sodium carboxymethyl cellulose composite film, *Ultrason. Sonochem.* 72 (2021) 105447.
- [19] X. Liang, S.Y. Feng, S. Ahmed, W. Qin, Y.W. Liu, Effect of potassium sorbate and ultrasonic treatment on the properties of fish scale collagen/polyvinyl alcohol composite film, *Molecules* 24 (13) (2019) 2363.
- [20] J.W. Lee, S.M. Son, S.I. Hong, Characterization of protein-coated polypropylene films as a novel composite structure for active food packaging application, *J. Food Eng.* 86 (4) (2008) 484–493.
- [21] S. Li, Y. Jiang, Y. Zhou, R. Li, Y. J. Jiang, M.D. Alomgir-Hossen, J. Dai, W. Qin, Y. Liu, Facile fabrication of sandwich-like anthocyanin/chitosan/lemongrass essential oil films via 3D printing for intelligent evaluation of pork freshness, *Food Chem.* 370 (2022).
- [22] P.P. Borah, P. Das, L.S. Badwaik, Ultrasound treated potato peel and sweet lime pomace based biopolymer film development, *Ultrason. Sonochem.* 36 (2017) 11–19.
- [23] L.M. Devi, C. Lalnunthari, L.S. Badwaik, Direct transformation of muskmelon seeds meal into biodegradable films and their characterization, *J. Polym. Environ.* 27 (3) (2019) 456–463.
- [24] J. Fang, R. Shi, Z. Meng, Y. Jiang, Z. Qin, Q. Zhang, Y. Qin, J. Tan, W. Bai, The interaction effect of catalyst and ash on diesel soot oxidation by thermogravimetric analysis, *Fuel* 258 (2019) 116151.
- [25] Q.Q. Yan, H.X. Hou, P. Guo, H.Z. Dong, Effects of extrusion and glycerol content on properties of oxidized and acetylated corn starch-based films, *Carbohydr. Polym.* 87 (1) (2022) 707–712.
- [26] Z.L. Yu, F.K. Alsammarraie, F.X. Nayigiziki, W. Wang, B. Vardhanabhuti, A. Mustapha, M.S. Lin, Effect and mechanism of cellulose nanofibrils on the active functions of biopolymer-based nanocomposite films, *Food Res. Int.* 99 (2017) 166–172.
- [27] W.J. Cheng, J.C. Chen, D.H. Liu, X.Q. Ye, F.S. Ke, Impact of ultrasonic treatment on properties of starch film-forming dispersion and the resulting films, *Carbohydr. Polym.* 81 (3) (2010) 707–711.
- [28] C. Colodel, L.C. Vriesmann, C.L.D. Petkowicz, Rheological characterization of a pectin extracted from ponkan (*Citrus reticulata* blanco cv. ponkan) peel, *Food Hydrocolloids* 94 (2019) 326–332.
- [29] K. Cruz-Diaz, Á. Cobos, M.E. Fernández-Valle, O. Díaz, M.I. Cambero, Characterization of edible films from whey proteins treated with heat, ultrasounds and/or transglutaminase. Application in cheese slices packaging, *Food Packaging Shelf Life* 22 (C) (2019) 100397.
- [30] P.J.P. Espitia, W.X. Du, R.D. Avena-Bustillos, N.D.F. Soares, T.H. McHugh, Edible films from pectin: physical-mechanical and antimicrobial properties – a review, *Food Hydrocolloids* 35 (2014) 287–296.
- [31] K.S. Suslick, G.J. Price, Applications of ultrasound to materials chemistry, *Cheminform* 29 (1) (1999) 295–326.
- [32] H.J. Bae, D.O. Darby, R.M. Kimmel, H.J. Park, W.S. Whiteside, Effects of transglutaminase-induced cross-linking on properties of fish gelatin-nanoclay composite film, *Food Chem.* 114 (1) (2009) 180–189.
- [33] E. Marcuzzo, D. Peressini, F. Debeaufort, A. Sensidoni, Effect of ultrasound treatment on properties of gluten-based film, *Innovat. Food Sci. Emerg. Technol.* 11 (3) (2010) 451–457.
- [34] H.J. Bae, H.J. Park, S.I. Hong, Y.J. Byun, D.O. Darby, R.M. Kimmel, W. S. Whiteside, Effect of clay content, homogenization RPM, pH, and ultrasonication on mechanical and barrier properties of fish gelatin/montmorillonite nanocomposite films, *Lwt-Food Sci. Technol.* 42 (6) (2009) 1179–1186.
- [35] I. Marcet, C. Alvarez, B. Paredes, M. Rendueles, M. Díaz, Transparent and edible films from ultrasound-treated egg yolk granules, *Food Bioprocess Technol.* 11 (4) (2017) 735–747.
- [36] V. Del-Valle, P. Hernández-Muñoz, A. Guarda, M.J. Galotto, Development of a cactus-mucilage edible coating (*Opuntia ficus indica*) and its application to extend strawberry (*Fragaria ananassa*) shelf-life, *Food Chem.* 91 (4) (2005) 751–756.
- [37] A. Salem, O. Abdelhedi, H. Kchaou, N. Kakhfakh, M. Nasri, M. Jridi, N. Zouari, F. Debeaufort, The effects of agar addition and ultrasound treatment on thermomechanical and physical properties of smooth hound (*Mustellus mustellus*) skin gelatin film, *J. Food Meas. Charact.* 15 (3) (2021) 2211–2219.
- [38] T. Zhong, R. Huang, S.Y. Sui, Z.X. Lian, X.X. Sun, A.J. Wan, H.L. Li, Effects of ultrasound treatment on lipid self-association and properties of methylcellulose/stearic acid blending films, *Carbohydr. Polym.* 131 (2015) 415–423.
- [39] U.V. Brodnjak, Improvement of physical and optical properties of chitosan-rice starch films pre-treated with ultrasound, *Bul. Chem. Commun.* 49 (4) (2017) 859–867.
- [40] M.J. Fabra, M. Martínez-Sanz, L.G. Gomez-Mascaraque, J.M. Coll-Marques, J. C. Martínez, A. Lopez-Rubio, Development and characterization of hybrid corn starch-microalgae films: effect of ultrasound pre-treatment on structural, barrier and mechanical performance, *Algal Res.-Biomass Biofuels Bioprod.* 28 (2017) 80–87.
- [41] Y.J. Oh, B.A. Nam, Preparation and characterization of Cu:SiO₂ aerogel films, *Solid State Sci.* 13 (8) (2011) 1579–1583.
- [42] I. Marcet, C. Alvarez, B. Paredes, M. Rendueles, M. Diaz, Transparent and edible films from ultrasound-treated egg yolk granules, *Food Bioprocess Technol.* 11 (4) (2018) 735–747.
- [43] D. Lin, W. Zhou, Q. He, B. Xing, Z. Wu, H. Chen, et al., Study on preparation and physicochemical properties of hydroxypropylated starch with different degree of substitution under microwave assistance, *Int. J. Biol. Macromol.* 125 (2018) 290–299.
- [44] C. Demetgul, N. Beyazit, Synthesis, characterization and antioxidant activity of chitosan-chromone derivatives, *Carbohydr. Polym.* 181 (2018) 812–817.
- [45] Y. Wang, S. Yi, R. Lu, D.E. Sameen, S. Ahmed, J. Dai, W. Qin, S. Li, Y. Liu, Preparation, characterization, and 3D printing verification of chitosan/halloysite nanotubes/tea polyphenol nanocomposite films, *Int. J. Biol. Macromol.* 166 (2021) 32–44.
- [46] D.A. Cuevas-Acuna, S. Ruiz-Cruz, J.L. Arias-Moscoco, M.A. Lopez-Mata, P. B. Zamudio-Flores, S.E. Burruel-Ibarra, H.D. Santacruz-Ortega, Effects of the addition of ultrasound-pulsed gelatin to chitosan on physicochemical and antioxidant properties of casting films, *Polym. Int.* 69 (4) (2020) 423–428.
- [47] D. Lin, Y. Yang, J. Wang, W. Yan, Z. Wu, H. Chen, Q. Zhang, D. Wu, W. Qin, Z. Tu, Preparation and characterization of TiO₂-Ag loaded fish gelatin-chitosan antibacterial composite film for food packaging, *Int. J. Biol. Macromol.* 154 (2020) 123–133.
- [48] F. Bi, X. Zhang, J. Liu, H. Yong, L.u. Gao, J. Liu, Development of antioxidant and antimicrobial packaging films based on chitosan, D-α-tocopheryl polyethylene glycol 1000 succinate and silicon dioxide nanoparticles, *Food Packaging Shelf Life* 24 (2020) 100503.
- [49] C.L. Pan, J.Q. Qian, J. Fan, H. Guo, L.H. Gou, H.Y. Yang, C.H. Liang, Preparation nanoparticle by ionic cross-linked emulsified chitosan and its antibacterial activity, *Colloids Surf. A-Physicochem. Eng. Aspects* 568 (2019) 362–370.
- [50] B. Tian, D. Xu, J. Cheng, Y. Liu, Chitosan-silica with hops β-acids added films as prospective food packaging materials: preparation, characterization, and properties, *Carbohydr. Polym.* 272 (4) (2021) 118457.

- [51] A.A. Menazea, N.S. Awwad, Antibacterial activity of TiO₂ doped ZnO composite synthesized via laser ablation route for antimicrobial application, *J. Mater. Res. Technol.* 9 (4) (2020) 9434–9441.
- [52] S. Das, P. Pandey, S. Mohanty, S.K. Nayak, Evaluation of biodegradability of green polyurethane/nanosilica composite synthesized from transesterified castor oil and palm oil based isocyanate, *Int. Biodeterior. Biodegrad.* 117 (2017) 278–288.
- [53] S. Kubowicz, A.M. Booth, Biodegradability of plastics: challenges and misconceptions, *Environ. Sci. Technol.* 51 (21) (2017) 12058–12060.
- [54] A.R. Deshmukh, H. Aloui, C. Khomlaem, A. Negi, J.-H. Yun, H.-S. Kim, B.S. Kim, Biodegradable films based on chitosan and defatted *Chlorella* biomass: functional and physical characterization, *Food Chem.* 337 (2021) 127777.
- [55] A. Oberlntner, M. Bajić, G. Kalčíková, B. Likozar, U. Novak, Biodegradability study of active chitosan biopolymer films enriched with *Quercus* polyphenol extract in different soil types, *Environ. Technol. Innovation* 21 (2021).
- [56] R.L. Marcondes, V.P. Lima, F.J. Barbon, C.P. Isolan, M.A. Carvalho, M.V. Salvador, A.F. Lima, R.R. Moraes, Viscosity and thermal kinetics of 10 preheated restorative resin composites and effect of ultrasound energy on film thickness, *Dent. Mater.* 36 (10) (2020) 1356–1364.
- [57] C.J. Cabello-Alvarado, Z.V. Quinones-Jurado, V.J. Cruz-Delgado, C.A. Avila-Orta, Pigmentation and degradative activity of TiO₂ on polyethylene films using masterbatches fabricated using variable-frequency ultrasound-assisted melt-extrusion, *Materials (Basel)* 13 (17) (2020) 3855.
- [58] A. Soleimani Dorcheh, M.H. Abbasi, Silica aerogel; synthesis, properties and characterization, *J. Mater. Process. Technol.* 199 (1–3) (2008) 10–26.
- [59] W. Zhang, J.L. Zhang, Q.X. Jiang, W.S. Xia, Physicochemical and structural characteristics of chitosan nanopowders prepared by ultrafine milling, *Carbohydr. Polym.* 87 (1) (2012) 309–313.
- [60] P.M. Rahman, V.M.A. Mujeeb, K. Muraleedharan, S.K. Thomas, Chitosan/nano ZnO composite films: enhanced mechanical, antimicrobial and dielectric properties, *Arabian J. Chem.* 11 (1) (2018) 120–127.
- [61] J.F. Rubilar, R.M.S. Cruz, H.D. Silva, A.A. Vicente, I. Khmelinskii, M.C. Vieira, Physico-mechanical properties of chitosan films with carvacrol and grape seed extract, *J. Food Eng.* 115 (4) (2013) 466–474.
- [62] J. Ahmed, M. Mulla, Y.A. Arfat, T.L.A. Thai, Mechanical, thermal, structural and barrier properties of crab shell chitosan/graphene oxide composite films, *Food Hydrocolloids* 71 (2017) 141–148.
- [63] P.P. Zuo, H.F. Feng, Z.Z. Xu, L.F. Zhang, Y.L. Zhang, W. Xia, W.Q. Zhang, Fabrication of biocompatible and mechanically reinforced graphene oxide-chitosan nanocomposite films, *Chem. Cent. J.* 7 (1) (2013) 39.
- [64] Z. Mazrouei-Sebdani, A. Khoddami, H. Hadadzadeh, M. Zarrebini, A. Karimi, F. Shams-Ghahfarokhi, The effect of the nano-structured aerogel powder on the structural parameters, water repellency, and water vapor/air permeability of a fibrous polyester material, *Mater. Chem. Phys.* 177 (2016) 99–111.
- [65] M.N. Muralidharan, K.P. Shinu, A. Seema, Optically triggered actuation in chitosan/reduced graphene oxide nanocomposites, *Carbohydr. Polym.* 144 (2016) 115–121.
- [66] M. Yadav, S. Ahmad, Montmorillonite/graphene oxide/chitosan composite: synthesis, characterization and properties, *Int. J. Biol. Macromol.* 79 (2015) 923–933.
- [67] Z. Wu, Y. Huang, L. Xiao, D. Lin, Y. Yang, H. Wang, Y. Yang, D. Wu, H. Chen, Q. Zhang, W. Qin, S. Pu, Physical properties and structural characterization of starch/polyvinyl alcohol/graphene oxide composite films, *Int. J. Biol. Macromol.* 123 (2019) 569–575.
- [68] S. Hajji, H. Kchaou, I. Bkhairia, R. Ben Slama-Ben Salem, S. Boufi, F. Debeaufort, M. Nasri, Conception of active food packaging films based on crab chitosan and gelatin enriched with crustacean protein hydrolysates with improved functional and biological properties, *Food Hydrocolloids* 116 (2021) 106639.
- [69] S. Sešljija, A. Nešić, J. Ružić, M. Kalagasidis Krusić, S. Veličković, R. Avolio, G. Santagata, M. Malinconico, Edible blend films of pectin and poly(ethylene glycol): preparation and physico-chemical evaluation, *Food Hydrocolloids* 77 (2018) 494–501.